J. Fluid Mech. (2001), *vol.* 433, *pp.* 315–328. Printed in the United Kingdom

Some steady axisymmetric vortex flows past a sphere

By ALAN ELCRAT[1], BENGT FORNBERG[2] AND KENNETH MILLER[1]

[1]Department of Mathematics, Wichita State University, Wichita, KS 67260, USA
[2]Department of Applied Mathematics, University of Colorado, Boulder, CO 80309, USA

(Received 22 March 2000 and in revised form 30 October 2000)

Steady, inviscid, axisymmetric vortex flows past a sphere are obtained numerically as solutions of a partial differential equation for the stream function. The solutions found include vortex rings, bounded vortices attached to the sphere and infinite vortex tubes. Four families of attached vortices are described: vortex wakes behind the sphere, spherically annular vortices surrounding the spherical obstacle (which can be given analytically), bands of vorticity around the sphere and symmetric pairs of vortices fore and aft of the sphere. Each attached vortex leads to a one-parameter family of vortex rings, analogous to the connection between Hill's spherical vortex and the vortex rings of Norbury.

1. Introduction

We are concerned here with steady, inviscid, axisymmetric flow past a sphere, the flow uniform at infinity. We consider flows in which there is a single vortex (or possibly two symmetrically placed vortices) in equilibrium with the sphere. There are three distinct types of vortices to be considered: vortex rings, bounded vortices attached to the sphere, and vortex 'tubes' extending to infinity along the axis. In the course of the paper we will describe several families of each type of vortex.

In general one can expect several families of inviscid vortex flows past a body of given shape, and can presume that a member of these families can be picked out using high Reynolds number asymptotics of the steady Navier–Stokes equations. This problem has been studied extensively, see, for example, Smith (1985), Peregrine (1985), Chernyshenko (1988) and Chernyshenko & Castro (1993). In the present work we have fixed ideas by considering only flow past the simplest body, a sphere, and have made an attempt to find all possible steady, inviscid flows with a single vortex. Apart from the appeal of knowing the mathematical possibilities, this provides a catalogue of possible limits, using different boundary conditions, for the steady Navier–Stokes equations. In addition, the Batchelor model may be a reasonable compromise between accuracy and simplicity when a vortex is trapped in the vicinity of a body, see Bunyakin, Chernyshenko & Stepanov (1998).

If we introduce a Stokes' stream function ψ for the flow,

$$u = \frac{1}{r}\psi_r, \qquad v = -\frac{1}{r}\psi_z,$$

u, v being the components of velocity in the axial and radial directions, then the

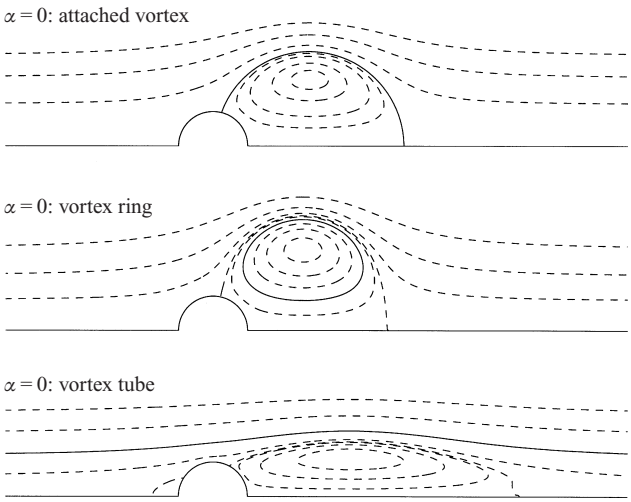

FIGURE 1. Examples of the three types of vortices obtained. The boundary of the vortex support, the streamline $\psi = \alpha$, is shown by a solid line. Other flow lines are dashed. The flow is from left to right in the far field. $\psi = 0$ on the axis and the boundary of the sphere. For all three flows $\omega = 1$. Values of α are $0, -0.6$ and 0.47 respectively.

vorticity vector is given by $(0, -L\psi/r, 0)$ in cylindrical coordinates, where

$$L\psi = r\left(\frac{1}{r}\psi_r\right)_r + \psi_{zz}.$$

We assume that outside the vortex region the flow has velocity $U = 1$ in the axial direction ($\psi \sim \frac{1}{2}r^2$) at infinity.

Steady flows result if

$$L\psi = \omega r^2 f(\psi) \tag{1.1}$$

for some function f. We will assume that $f(\psi) = 1 - H(\psi - \alpha)$, where H is the Heaviside function and α is the value of the stream function on the boundary of the vortex. We have introduced the vortex strength parameter $\omega > 0$ as a factor for convenience. The vorticity in the vortex region is then $(0, -\omega r, 0)$. It should be noted that flows obtained by solving equation (1.1) generally have only a single vortex region; if there are multiple regions, the values of both ω and α are the same for all regions. (In general the functional relationship between vorticity and stream function in a steady, axisymmetric flow need not be global.) It is also noted that solutions of (1.1) are continuously differentiable, so there are no vortex sheets.

The meridional plane cross-section of the vortex support for each solution is $\{(r, z) : \psi(r, z) < \alpha\}$. Taking the value of ψ on the surface of the sphere to be 0, the three classes of vortices – attached, detached (vortex rings), and tubes – correspond to α being zero, negative and positive respectively. For $\alpha < 0$, $-\alpha$ is the flux constant: $1/2\pi$ times the flux of the flow between the axis and the boundary of the vortex. Figure 1 shows examples of the three classes of vortices. These examples will be discussed further in § 3.

For fixed α and ω the partial differential equation (1.1) cannot be expected to have a unique solution. For $\alpha = 0$ we have found four distinct one-parameter families of vortices: vortex wakes behind the sphere (one of which is shown in figure 1), spherically annular vortices surrounding the sphere (given analytically in § 4), bands

of vorticity around the circumference of the sphere, and symmetric regions of vortices fore and aft of the sphere. Vortices in the first family approach the spherical vortex of Hill (1894) as the size of the vortex region, compared to the sphere, becomes large. These four families of attached vortices will be discussed further in § 3.

In the case of vortex rings translating in free space, Norbury (1973) has given a family, parametrized by core radius, which connects Hill's vortex to thin rings. We give analogous results for the various attached vortices described above and stationary vortex rings in equilibrium with the sphere: each attached vortex leads to a fixed-circulation family of vortex rings, parametrized by the flux constant. In a somewhat similar fashion, described in § 3, certain attached vortices can be perturbed to obtain families of vortex tubes.

There is a close analogy between the results presented here and our recent results for two-dimensional flows past a circular cylinder given in Elcrat *et al.* (2000). In that work equilibrium positions for point vortices play an important role: a fixed-circulation vortex family approaches a point vortex as the flux constant approaches infinity. However, there is no dynamically valid analogue of a stationary point vortex for axisymmetric flow: infinitesimal vortex rings propagate with infinite speed (Saffman 1992, p. 36). Kelvin's formula for a thin vortex ring indicates that the radius of a vortex ring may be expected to go to infinity as the flux constant goes to infinity, and this seems to be borne out in our calculations.

In Fornberg (1988) Hill's spherical vortex arose in the study of solutions of the steady Navier–Stokes equations for high-Reynolds-number flow past a sphere. A rapidly convergent Newton's method was used to avoid naturally occurring instabilities, and a wake, with size growing slowly with Reynolds number, was found which asymptotes to Hill's spherical vortex. Those calculations indicate that the first family of attached vortices obtained here closely approximates high-Reynolds-number viscous wakes. The questions of time stability of the solutions of the Euler equations obtained here and their relation to solutions of the steady Navier–Stokes equations are natural ones to raise. However, we do not deal with these questions here.

Steady flows are found here by numerically solving a partial differential equation for the stream function. We use a non-Newton-based iterative scheme, similar to that employed in Elcrat *et al.* (2000). However, there are some important differences in how the scheme is implemented here compared with that work. In particular, the differential operator in the present study is not formally self-adjoint, so an alternative to the fast Fourier transform is required in solving the linear equation at each iterative step.

2. Numerical procedures

By symmetry we need only consider the upper half of the meridional plane. Introducing the complex variable $q = z + \mathrm{i}r$, we make the change of variables $\zeta = \xi + \mathrm{i}\eta = \mathrm{i}\ln q$. Equation (1.1) then transforms to

$$\tilde{L}\psi = (\omega \mathrm{e}^{4\eta} \sin^2 \xi) f(\psi) \tag{2.1}$$

where $\tilde{L}$ is the differential operator

$$\tilde{L}\psi = \psi_{\xi\xi} + \psi_{\eta\eta} - (\cot \xi)\psi_{\xi} - \psi_{\eta}.$$

If the flow domain is the exterior of a sphere of radius one, we obtain an infinite strip in the ζ-plane given by $-\pi < \xi < 0,\ 0 < \eta < \infty$. The boundary condition on the three sides of the strip is $\psi = 0$.

In order to get a finite computational domain we truncate at some larger sphere of radius R, and this truncates the strip at height $\ln R$. We next describe how we obtain the boundary condition that we impose on the top of the truncated strip. Assuming that the vortex is inside a sphere of radius $R_1 < R$, then $L\psi = 0$ outside this sphere. Solutions of $L\psi = 0$ can be expressed as eigenfunction expansions in terms of basis functions that correspond to spherical harmonics for the velocity potential, see Batchelor (1967, p. 450). These basis functions are

$$\phi_{-n} := \frac{1}{n+1}\rho^{n+1}(1-\mu^2)\frac{\mathrm{d}P_n(\mu)}{\mathrm{d}\mu}$$

and

$$\phi_n := -\frac{1}{n}\frac{1}{\rho^n}(1-\mu^2)\frac{\mathrm{d}P_n(\mu)}{\mathrm{d}\mu},$$

$n \geqslant 1$, where ρ is the spherical radial coordinate, $\rho^2 = z^2 + r^2, \mu = z/\rho$ and P_n is the Legendre polynomial of order n. Uniform flow at infinity implies that the terms $\phi_{-n}, n > 1$, do not occur in the expansion. Also, the stream function ψ_0 for irrotational flow past the unit sphere with velocity one at infinity is

$$\psi_0 = \tfrac{1}{2}r^2(1-\rho^{-3}) = \phi_{-1} + \tfrac{1}{2}\phi_1.$$

In spherical coordinates the basis functions $\phi_n, n \geqslant 1$, satisfy

$$\frac{\partial \phi_n}{\partial \rho} + \frac{n}{\rho}\phi_n = 0.$$

Assuming that we can neglect coefficients of ϕ_n for $n > 2$, we obtain the boundary condition

$$\frac{\partial \Psi}{\partial \rho} + \frac{2}{\rho}\Psi = 0 \tag{2.2}$$

on the sphere of radius R, where $\Psi = \psi - \psi_0$. (The validity of this assumption can be checked after the fact by increasing R, and we do this in our computations.) Under the coordinate transformation this yields the Robin-type boundary condition

$$\frac{\partial \Psi}{\partial \eta} + 2\Psi = 0$$

on the top of the truncated strip.

One can imagine a more sophisticated procedure in which the condition satisfied by each ϕ_n is imposed on a discretization of the equation corresponding to a non-local condition on ψ. This was done in our previous work on two-dimensional flows, but did not turn out to be necessary here.

We discretize the problem using a uniform grid on the rectangle

$$-\pi \leqslant \xi \leqslant 0, \qquad 0 \leqslant \eta \leqslant \ln R$$

in the ζ-plane. Solutions to the nonlinear equation (2.1) are obtained using iterations to be described below, and the linear equations arising in the iterative procedure are solved using the multigrid package MUDPACK, Adams (1989).

There are two parameters, ω and α, in the problem being studied. In Elcrat *et al.* (2000) in order to obtain convergence of the iterative procedure we introduced an additional parameter A, the area of the vortex region, and determined ω as part of the solution. Constraining the area (or some other geometric measure of the vortex size) ensures numerical convergence irrespective of any possible physical instabilities. In the

axisymmetric problem rather than area we use the parameter M, where $M = \int_S r\mathrm{d}A$ is the first moment with respect to the axis of symmetry of the cross-section S of the vortex region in the meridional half-plane. M is used instead of A because the circulation κ of a vortex in axisymmetric flow is $\kappa = \omega M$.

Given M and α, the basic iteration we use takes the form

$$L\psi_{n+1} = \omega_n r^2 f(\psi_n) \tag{2.3}$$

where ω_n is adjusted in an inner iteration so that the moment of the approximate vortex region $S_{n+1} = \{\psi_{n+1} < \alpha\}$ is equal to M to within some prescribed tolerance. (We generally set this tolerance equal to the area of one grid rectangle in the computational domain.) An initial guess ω_0 and an initial guess S_0 for the vortex region are given. The right-hand side of (2.3) in the first iterative step is $\omega_0 r^2$ on S_0 and 0 off S_0.

The moment of S_{n+1} is computed by adding together the contributions to the moment of the transformed grid rectangles that intersect S_{n+1}. If the images of all four corners of the grid rectangle $[\xi_1, \xi_2] \times [\eta_1, \eta_2]$, are contained in S_{n+1} the moment can be computed exactly:

$$\int_{\eta_1}^{\eta_2} \int_{\xi_1}^{\xi_2} (-\sin\xi \exp(3\eta))\mathrm{d}\xi\mathrm{d}\eta.$$

If some but not all corners of a grid rectangle are in S_{n+1} then as in Elcrat *et al.* (2000) we use linear interpolation on the sides of the rectangle where $\psi_{n+1} - \alpha$ changes sign to approximate the fraction of the area of the grid rectangle that is in S_{n+1}. That fraction of the moment of the transformed grid rectangle is then taken as the contribution of that rectangle to the total moment.

The iterations are continued until the set of grid points in S_{n+1} is the same as the set of grid points in S_n. The inner iterations used to determine ω_n are done using the secant method with stopping criterion $|\omega_{n,j+1} - \omega_{n,j}| < h^2$, where h is the mesh width in the ζ-plane.

3. Results

We will give examples that represent the various solutions we have found. The graphs which follow show cross-sections of the vortex in the upper half of the meridional plane. The differential equation (1.1) and the boundary conditions are invariant under the transformation $z \to -z$, so a non-symmetric vortex always has a reflected twin. These reflected solutions will not be discussed further. The radius of the spherical obstacle is taken to be one throughout.

3.1. *Attached vortices*

For attached vortices $\alpha = 0$ and M is a parameter. As noted earlier, solutions to the differential equation (1.1) are not unique. As discussed further in this subsection, we have in fact found four families of solutions, parametrized by M, when $\alpha = 0$. Numerically these different families are obtained by taking different initial guesses for the vortex region. One of the features of our solution method is that an *a priori* 'guess' as to where a steady vortex might occur can be used as the initial set S_0 for the iterations.

First we have found a set of vortices that have the character of a separation bubble behind the sphere. These vortices may be thought of as perturbations of Hill's

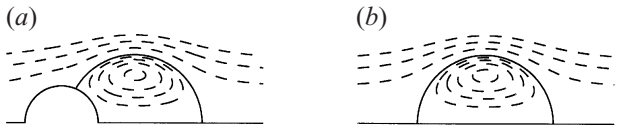

FIGURE 2. Streamlines plot for (*a*) flow past a sphere with an attached vortex with $M = 4$, $\omega = 2.2$, and (*b*) Hill's spherical vortex of radius 1.85, which has the same value of ω.

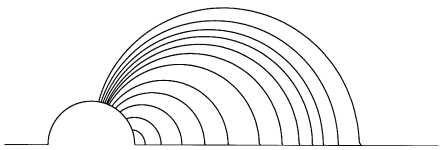

FIGURE 3. Attached ($\alpha = 0$) trailing vortices.
Values of M are 0.01, 0.1, 0.4, 1, 2, 4, 6, 8, 10, 12, 15 and 20.

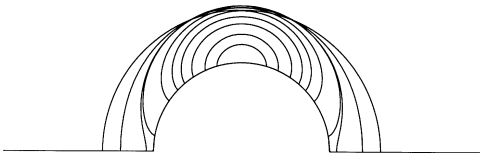

FIGURE 4. Attached vortex bands. Values of M are 0.1, 0.25, 0.5, 0.75, 1, 1.25, 1.52, 1.56, 1.8, 2.

spherical vortex. Streamlines for the flow when $M = 4$ are shown in figure 2 along with the streamlines for the comparable Hill's vortex. Numerical solutions for viscous flow past a sphere obtained previously in Fornberg (1988) suggest that solutions in this family closely approximate high-Reynolds-number viscous wakes. Solutions in this family for several values of M are shown in figure 3.

It is noted that to within the computational accuracy of our numerical results (approximately $2h$ where h is the grid spacing), each vortex boundary is indistinguishable from a section of a sphere. While it is to be expected that for large M the vortices should be nearly spherical, that the boundaries are also apparently spherical even for small M is perhaps surprising.

For a second family of solutions the boundaries of the converged solutions are spheres concentric with the spherical obstacle. In fact we will show in § 4 that these solutions can be given analytically, generalizing Hill's analytic solution.

A third family of attached vortices is shown in figure 4. For small values of M the vortex is a small band around the circumference of the sphere, as shown by a small region at the top of the semicircle in the meridional plane. As M increases the vortex expands and surrounds the sphere at approximately $M = 1.55$. As M increases further the vortex attains an almost spherical shape at approximately $M = 2$.

For solutions in the fourth family of attached vortices, figure 5, there are two symmetric regions of vorticity, fore and aft of the sphere. The value of M for this family ranges from 0 to about 4.65. As M approaches this maximal value the attachment points in the meridional cross-section approach the top of the semi-circle. As discussed further in the next subsection, in contrast to the two-dimensional case we were not able to continue this family to include vortices that completely surround the obstacle.

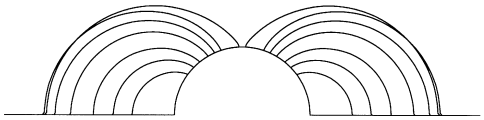

FIGURE 5. Solutions with two symmetric attached vortex regions. Values of M are 0.2, 0.5, 1, 2, 3, 4, 4.65.

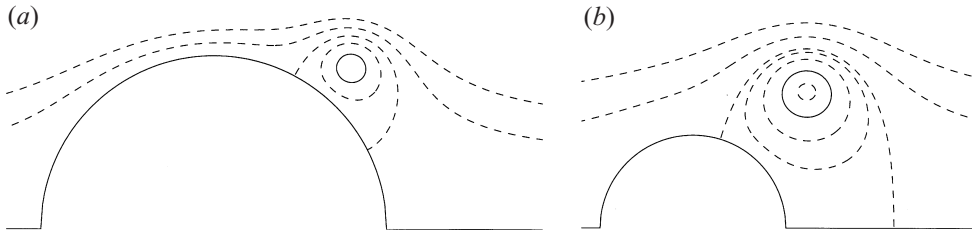

FIGURE 6. Streamline plot for flow with (*a*) $\kappa = 2$ and $\alpha = -0.3$; and (*b*) $\kappa = 5$ and $\alpha = -1.04$.

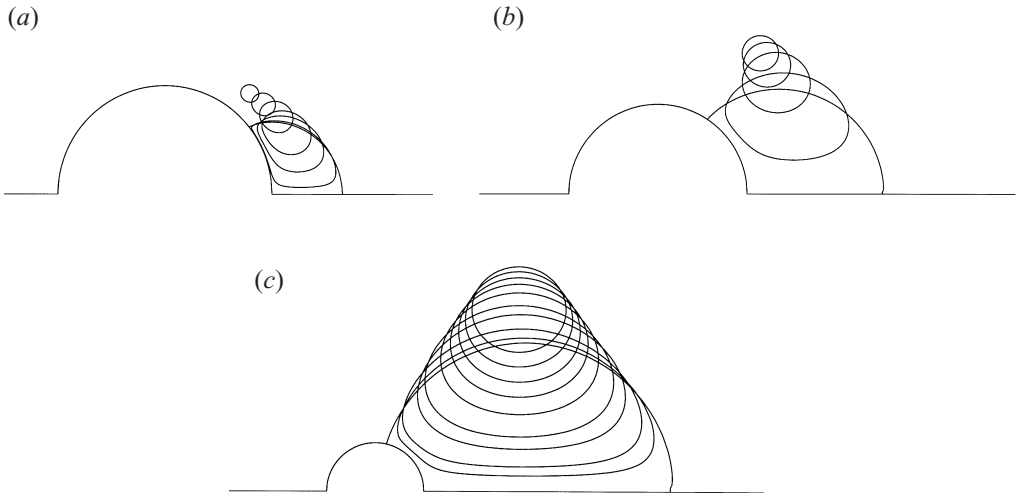

FIGURE 7. Vortex rings trailing the sphere, with (*a*) $\kappa = 2$, values of α are 0, -0.002, -0.02, -0.06, -0.14, -0.22, -0.30; (*b*) $\kappa = 5$, values of α are 0, -0.1, -0.59, -1.04 and -1.43; (*c*) $\kappa = 15$, values of α are 0, -0.08, -0.2, -0.6, -1.98, -2.97, -3.98, -5.17, and -6.51.

3.2. *Vortex rings*

Taking $\alpha < 0$ yields vortex rings (or detached vortices) as solutions. Norbury (1972) described a family of steady vortex rings as perturbations of Hill's spherical vortex and numerically continued the family to small-cross-section vortices in Norbury (1973). We can similarly perturb any of the attached vortices described above to obtain vortex rings.

Streamline plots for two vortex rings are shown in figures 6(*a*) and 6(*b*). The shape of the stagnation streamline in figure 6(*b*) is quite similar to that shown in figure 4 of Norbury (1973) for a vortex ring in the full space with a comparable ratio of vortex core radius to ring radius.

We organize the various vortex rings we have found by presenting fixed-circulation families of vortex rings, parametrized by $\alpha < 0$, one such family for each of the attached vortices described in the previous subsection. Figures 7(*a*), 7(*b*) and 7(*c*)

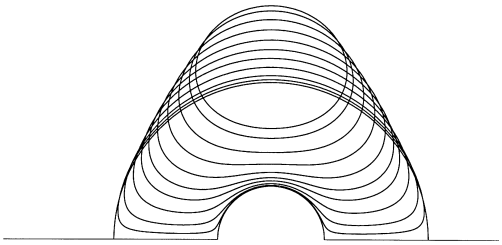

FIGURE 8. Vortex rings perturbed off the concentric spherical attached vortex, with $\kappa = 15$. Values of α are $0, -0.005, -0.03, -0.1, -0.22, -0.36, -0.6, -1, -1.6, -2.4, -3$.

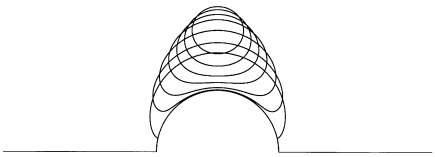

FIGURE 9. Vortex rings perturbed off an attached vortex band, $\kappa = 7$. Values of α are $0, -0.02, -0.1, -0.3, -0.58, -1, -1.58$.

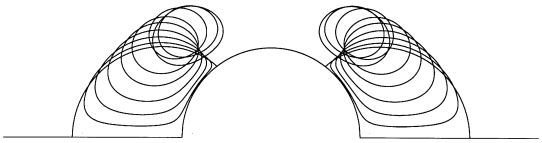

FIGURE 10. Vortex ring pairs, with $\kappa = 8$. Values of α go from 0 to -0.43, then increase again to -0.27 as the vortex regions move toward the vertical axis.

show sequences of vortex rings perturbed from trailing attached vortices for three values of circulation κ.

The streamline plots shown in figure 6(a, b) are for vortices in figure 7(a, b) respectively. Figures 8, 9 and 10 show sequences of rings associated with one case of each of the other three types of attached vortex as described in the preceding subsection.

Two algorithms were used to obtain these families. The first is an iterative procedure that uses the basic algorithm described at the end of § 2 at each iteration. Given α and M the basic algorithm determines an ω and corresponding solution to (1.1) with vortex circulation $\kappa(M) = \omega M$. If κ is prescribed we then use a nonlinear equation solving routine to vary M so as to solve $\kappa(M) = \kappa$. Note that there are three levels of iteration with this algorithm and a numerical solution of the partial differential equation (2.3) is required at each inner step. The second algorithm is much less computationally intensive: given κ and M (and hence ω) the equation

$$\tilde{L}\psi_{n+1} = (\omega e^{4\eta} \sin^2 \xi)(1 - H)(\psi_n - \alpha_n)$$

is solved once in each outer iteration. Then $\alpha = \alpha_{n+1}$ is varied in an inner iteration to satisfy the constraint on M. Unfortunately the much faster second algorithm was not successful in locating solutions for α close to 0. Starting from an attached vortex, as α decreases from 0 with κ fixed the value of M initially increases, then decreases. The second algorithm only found solutions on the portion of the family where M decreases. Thus the first algorithm had to be used to find solutions for an initial range of negative α.

In our previous work on two-dimensional vortices, structure was given to the set of

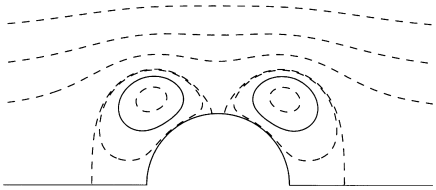

FIGURE 11. Streamline plot for flow with $\kappa = 8$ with vortex regions near the end of the family shown in figure 10. The stagnation points are near the top of the circle.

detached vortices by showing that for an attached vortex ($\alpha = 0$) there is a stationary point vortex ($\alpha = -\infty$) (or a symmetric point vortex pair) with the same circulation κ and a fixed-κ family of detached vortices parametrized by α joining the attached vortex to the point vortex. There is no analogue of a stationary point vortex for axisymmetric flow. Figures 7–9 suggest that, for fixed κ, as α decreases the vortex cross-section eventually assumes a nearly circular shape, bounded away from the axis, with cross-sectional area decreasing to 0 as $\alpha \to -\infty$. Also Kelvin's formula (Saffman 1992, p. 195) for a vortex ring

$$U \sim \frac{\kappa}{4\pi R}\left(\ln\left(\frac{8R}{a}\right) - \frac{1}{4}\right)$$

as $a/R \to 0$, where $U = 1$ is the propagation speed, R the ring radius, and a the core radius, indicates that R slowly goes to infinity as $\alpha \to -\infty$ with κ fixed, since $a \to 0$ and R is bounded away from 0 as $\alpha \to -\infty$.

It appears likely that starting with any vortex from one of the first three families of attached vortices, the corresponding fixed-circulation family of vortex rings exists for the entire range of $\alpha < 0$. However, as explained in § 3.4, we have encountered problems of resolution in computing small-cross-section vortices with our algorithm, these resolution problems increasing as the distance from the ring to the axis increases. So we were not able to compute solutions for large negative α. We can conjecture that as $\alpha \to -\infty$ the vortices in figure 7(*a–c*) approach the vertical axis through the centre of the sphere or eventually merge with the family centred on that axis, but we cannot take h small enough to conclusively show this. We also note that we are unable to resolve vortices for which the ratio of core radius to ring radius is so small as to obtain flows in which there is an interior stagnation point between the vortex and the axis. (Saffman (1992) indicates that this will occur when the ratio is less than 1/86 in the case of flow without an obstacle.)

For any of the double attached vortices in figure 5 the corresponding family (figure 10) of vortex rings was extended for only a small range of $\alpha < 0$. An obstruction to further continuation of the family appears to occur as the stagnation points on the semi-circle in the meridional half-plane approach the top of the circle (see figure 11). This contrasts with the case of two-dimensional flow where similar flows with two regions of vorticity can be continued to contain flows in which the $\psi = 0$ streamline goes above the top of the circle (see figure 12 in Elcrat *et al.* (2000)). Such flows have a stagnation point on the vertical axis of symmetry. The axisymmetric analogue of an interior stagnation point would be an interior stagnation circle. We have found no steady axisymmetric flows with an interior stagnation circle near the sphere.

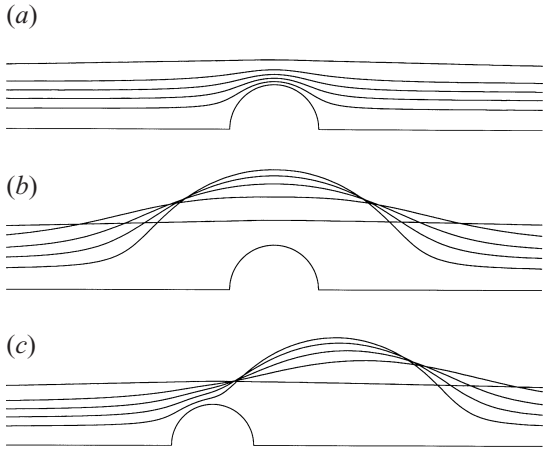

FIGURE 12. Vortex tubes, with $\omega = 1$: (*a*) perturbations of potential flow; (*b*) perturbations of the concentric spherical solution; (*c*) perturbations of a vortex in figure 3. Values of α are 0.1, 0.2, 0.3, 0.4 and 0.5.

3.3. *Vortex tubes*

Vortices with support extending to infinity along the axis of symmetry occur when $\alpha > 0$. Neither circulation nor moment is defined for unbounded vortices, so we use ω as the second prescribed parameter. As noted earlier, to obtain convergence we must constrain some geometric measure of the vortex size, and for that purpose we use area of the vortex in the computational domain in this case. The algorithm used is the same as the first algorithm described for obtaining vortex rings, with M replaced by area in the computational domain.

As described below, we have solutions which are perturbations of (*a*) potential flow, (*b*) the concentric spherical vortices and (*c*) the trailing vortices in figure 3. These three families are shown in figure 12(*a–c*) in the case $\omega = 1$. For all three families the continuation cannot be carried out past a maximal value of α which depends on ω. As in the case of two-dimensional flow, this maximal value is the same for all three families (four families counting the reflection of the third family).

For the $\alpha = 0$ vortex in the family shown in figure 12(*b*) each streamline $\psi = c$, $c < 0$ is a single simple closed curve: the stream function ψ has a unique minimum on the r-axis. As seen in figure 13 when $\alpha = 0.4$ the stream function has two minima: there are two rings of re-circulating fluid within a region of re-circulating fluid surrounding the sphere. When $\alpha = 0.49$ the two minima have become further separated and there are stagnation points on the sphere.

The lower streamline plot in figure 1 is for the $\alpha = 0.47$ vortex in the family shown in figure 12(*c*). As α increases from 0.47 to 0.5 in this family, the region of recirculating fluid in front of the sphere becomes larger and the region behind the sphere becomes smaller, so that the maximal $\alpha = 0.5$ solution is symmetric (with the same flow pattern as in figure 13*b*). For perturbations of potential flow, regions of re-circulating flow fore and aft of the sphere are not visible for $\alpha < 0.45$ with the resolution we have used. (See figure 14.) These regions increase rapidly in size as α increases from 0.48 to 0.5.

Analysis of similar axisymmetric flows in the full space indicates why there is a maximal value of α given ω. For a full-space axisymmetric flow with vortex tube $\{(z,r) : r < r_0\}$, velocity U for $r > r_0$ and velocity u_a on the axis, the stream function

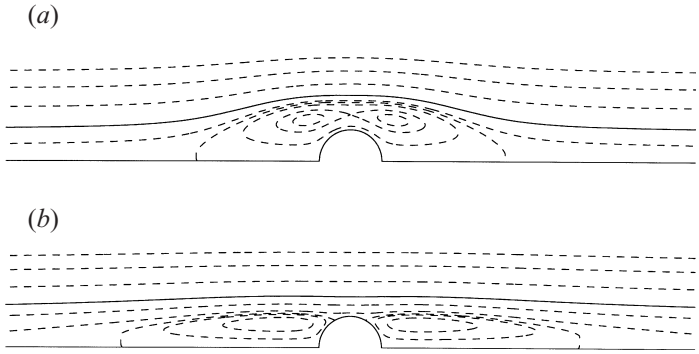

FIGURE 13. Streamline plots for vortices in the family given in figure 12*b*, for α equal to 0.4 (*a*) and (*b*) 0.49.

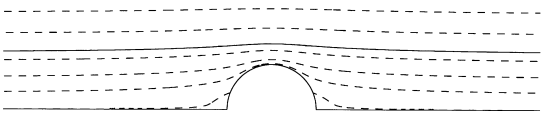

FIGURE 14. Streamline plot for the $\alpha = 0.48, \omega = 1$ perturbation of potential flow.

ψ is given by

$$\psi = \begin{cases} \frac{1}{2}u_a r^2 + \frac{1}{8}\omega r^4, & \psi < \alpha, \\ \frac{1}{2}Ur^2 + k, & \psi > \alpha, \end{cases}$$

with $\psi = \alpha$ when $r = r_0$. Differentiability implies $U^2 - u_a^2 = 2\alpha\omega$. The value of r_0 is given by $\omega r_0^2 = 2(U - u_a)$. Thus if $2\alpha\omega < U^2$ is satisfied there are two such tubes ($u_a > 0$ and $u_a < 0$). This accounts for two families with the same maximal α (given ω). In the presence of a sphere the third family (figure 12(*c*)) arises by matching a solution from the first family in the far-field upstream with a solution from the second family in the far-field downstream.

3.4. *Computational accuracy*

The validity of using the numerical boundary condition (2.2) on the truncating sphere was checked using a test problem for which an exact solution is known. The error was at the level of the truncation error of the discretization. The radius of the truncation sphere was squared from its original value of e^{π} (the rectangle in the parameter plane was doubled in height), and the effect was negligible.

Comparison of the numerical results with the analytic formula given in the next section for the concentric spherical family of solutions provides a check on the accuracy of the full routine. Generally when the routine converged to one of these vortices, the boundary of the converged solution agreed with the expected spherical boundary to within h in the computational domain, where h is the grid spacing.

We have used a rectangle of height π in the computational domain, and $h = \Delta\xi = \Delta\eta = 2^{-m}\pi$, with m an integer between 9 and 11. We can make an estimate of the accuracy of the solutions by noting the extent of variability of the computed solutions for different initial guesses. Considering the vortices shown in figure 3, the deviation in the computed points on the vortex boundary among the various computed solutions for a given M was observed to be at most $2h$ for $M < 15$. For $15 < M < 20$, this deviation was at most $3h$. Due to the exponential nature of the coordinate

transformation in the radial direction, the maximum error in the determination of the vortex boundaries in this family can be taken to be approximately $2h\rho$ for $M < 15$ ($3h\rho$ for $15 < M < 20$), where ρ is the spherical radial coordinate. Converged solutions were also checked by doubling the number of grid points.

Although the numerical procedure always converges, two kinds of 'phantom' solution were obtained but discarded because the solutions did not remain upon further grid refinement. First, at a given level of discretization h, we found nearly spherical downstream vortices with arbitrary centre z on the axis of symmetry for all $z > \bar{z}$, where $\bar{z}$ depends on M and h. However, with greater accuracy the value of $\bar{z}$ increases, i.e. the closest such downstream vortex moves further downstream. We conclude that any such far-downstream standing vortex could be eliminated if the precision were sufficiently great. Also, for vortex rings with small cross-section the computation becomes delicate. For fixed h, κ and small M, 'solutions' appear centred continuously along a nearly horizontal curve. When h is decreased however, this indeterminacy can be resolved. For example, consider the case $\kappa = 5.0$ and $M = 0.2$: the smallest vortex region shown in figure 7(b). With 2^9 grid points 'solutions' were found in which the centre of the vortex could be anywhere along a nearly horizontal curve. With 2^{10} grid points this continuum of 'solutions' broke into three pieces: the z-coordinate of the vortex centre varying in the interval $[0, 0.12]$ for the first piece, the interval $[0.85, 1.5]$ for the second piece and the interval $[2.4, \infty)$ for the third piece. With 2^{11} grid points these intervals reduced to $[0, 0.02]$, $[1.04, 1.21]$ and $[3.3, \infty)$ respectively. We conclude that there are actually only two solutions, one with centre on the vertical axis and one trailing vortex shown in figure 7(b), the third interval giving phantom solutions as discussed above. We note that the second smallest vortex shown in that figure is resolved to graphical accuracy with 2^{11} grid points and the next two vortices, $M = 0.5$ and $M = 0.7$ are resolved to graphical accuracy with 2^{10} and 2^9 grid points respectively. For any level of discretization, there will be similar problems of resolution if the vortex cross-section is too small or too far from either coordinate axis. This resolution problem is greater for axisymmetric flow than for the case of two-dimensional flow.

In comparison to procedures based on Newton's method, the numerical scheme used here has gained much in terms of ease of implementation, ease of use, and higher computational speed. However, although we observe a 'robust' linear rate of convergence to 'nearby' solutions in virtually all cases, we have not been able to demonstrate that convergence is guaranteed in every case when there is a physical solution near to a numerical guess. Hence, the fact that we have been unable to numerically connect the solution classes shown in figures 4 and 5 does not rule out the possibility of there existing a connecting branch of solutions.

4. An analytical solution generalizing Hill's spherical vortex

There are analogues of Hill's spherical vortex with a concentric solid spherical boundary. These were found numerically by our algorithm as discussed in § 3.1. Here we determine these solutions analytically. Let $\rho = \sqrt{r^2 + z^2}$ be the spherical radial coordinate. For any $b \geqslant 0$ and $\omega > 0$ we show that there is an explicit solution of

$$L\psi = \begin{cases} \omega r^2, & b < \rho < a \\ 0, & \rho > a \end{cases}$$

with $\psi = 0$, on $\rho = b$, for some uniquely determined $a > b$. Hill's vortices are obtained when $b = 0$.

We seek solutions to $L\psi = \omega r^2$ of the form $\psi = r^2 f(r^2 + z^2)$. This differential equation is satisfied if

$$10f'(t) + 4tf''(t) = \omega$$

for which the general solution is

$$f(t) = \tfrac{1}{10}\omega t + \tfrac{2}{3}c_1 t^{-3/2} - c_2.$$

Setting $\psi = 0$ on $\rho = a$ and solving for c_2 implies

$$r^{-2}\psi = \tfrac{1}{10}\omega(\rho^2 - a^2) + \tfrac{2}{3}c_1(\rho^{-3} - a^{-3}), \quad \rho < a. \tag{4.1}$$

For irrotational flow past a sphere of radius a with velocity U in the axial direction at infinity

$$r^{-2}\psi = \tfrac{1}{2}U(1 - a^3/\rho^3), \quad \rho > a. \tag{4.2}$$

The tangential velocities match at $\rho = a$ if

$$U = \tfrac{2}{15}a^2\omega - \tfrac{4}{3}c_1 a^{-3}. \tag{4.3}$$

(Hill's vortex is obtained if $c_1 = 0$.) If we now set $\psi = 0$ when $\rho = b$ in (4.1), solve for c_1 and substitute in (4.3), we obtain

$$\frac{U}{\omega} = \frac{2}{15}a^2 - \frac{1}{5}\frac{b^3(a+b)}{(a^2 + ab + b^2)}. \tag{4.4}$$

For fixed b the right-hand side of this equation is strictly increasing in a, vanishes for $a = b$ and goes to infinity with a. Thus for any positive U and ω there is a unique $a > b$ for which (4.1) and (4.2) give the solution. Alternatively, if for example a, b and U are given, ω can be determined by (4.4) to yield a solution given by (4.2) and

$$r^{-2}\psi = \frac{\omega}{10}\left((\rho^2 - a^2) + \frac{a^2 - b^2}{a^3 - b^3}(\rho^{-3} - a^{-3})\right), \quad b < \rho < a.$$

The circulation $\kappa = \omega M$ of these vortices has a limiting value of $6Ub$ as a approaches b. This follows from (4.4) and the formula $M = 2(a^3 - b^3)/3$ for the moment of the vortex cross-section in the meridional half-plane.

The vortices found in this section complement the 'Hill's vortices in a ball' given in Appendix B of Amick & Fraenkel (1986); there an outer spherical boundary was added to Hill's vortex, whereas here an inner spherical boundary has been added.

5. Conclusions

Euler flows often serve as basic building blocks for the understanding of more complex flow scenarios. In this study we have provided a collection of simple flows that significantly extends the known possible solutions of the steady Euler equations for flow past a spherical body.

Summarizing the flows obtained, we have described vortices attached to the body, vortex rings and infinite tubes of vorticity. Four families of attached vortices have been found. Each attached vortex can be perturbed to a fixed-circulation family of vortex rings parametrized by $\alpha < 0$ where $-\alpha$ is the flux constant. Some attached vortices can also be perturbed to $\alpha > 0$, yielding families of vortex tubes. One family of attached vortices approximates high-Reynolds-number viscous wakes behind the sphere. Within the accuracy of our computations the boundaries for this family of attached vortices appear to be sections of spheres.

These results have much in common with those for two-dimensional flow past a cylinder in Elcrat *et al.* (2000), but differ in some ways. In particular, for axisymmetric

flow there is no direct analogue of a stationary point vortex, and Kelvin's formula suggests that as α approaches $-\infty$ the vortex regions become small-cross-section rings with ring radius approaching infinity. However, the resolution of our computations does not allow us to obtain small-cross-section rings with large ring radius.

These results can be extended and generalized in several ways.

In Elcrat & Miller (2001) an existence theorem was proven for axisymmetric flows past a body in a finite channel. The mathematical techniques used there require flow in a bounded domain. It would be of great interest to adapt those techniques to the current problem. In another direction, the results in Elcrat & Miller (2001) can be generalized to flows with swirl, and it seems likely that the computational algorithm of the present paper can also be generalized to obtain rings with swirl.

The problem of obtaining the solutions obtained here as high-Reynolds-number limits of the steady Navier–Stokes equations was mentioned in the introduction. For no-slip boundary conditions, Fornberg (1988) has shown that a properly scaled Hill's vortex is the likely asymptotic limit. The question remains, however, if other, perhaps Reynolds number dependent, boundary conditions might lead to other limits (Saffman 1981). In particular a finite-sized Batchelor-type vortex of the kind computed here might arise from blowing or suction at the back of the sphere.

Finally the question of stability of our solutions as solutions of the time-dependent Euler equations deserves study. We can generally expect instability from the work of Pozrikidis (1986) on Hill's vortex, but the modes of instability are likely to be interesting and may be related to the questions raised in the previous paragraph.

REFERENCES

Adams, J. 1989 mudpack: Multigrid Fortran software for the efficient solution of linear elliptic partial differential equations. *Appl. Math. Comput.* **34**, 113–146.

Amick, C. & Fraenkel, L. 1986 The uniqueness of Hill's spherical vortex. *Arch. Rat. Mech. Anal.* **92**, 91–119.

Batchelor, G. 1967 *An Introduction to Fluid Dynamics*. Cambridge University Press.

Bunyakin, A., Chernyshenko, S. & Stepanov, G. 1998 High-Reynolds-number Batchelor-model asymptotics of a flow past an aerofoil with a vortex trapped in a cavity. *J. Fluid Mech.* **358**, 283–297.

Chernyshenko, S. 1988 The asymptotic form of the stationary separated circumfluence of a body at high Reynolds number. *Appl. Math. Mech.* **52**, 746 (*Prikl. Matem. Mekh.* **52**, 958–966).

Chernyshenko, S. & Castro, I. 1993 High-Reynolds-number asymptotics of the steady flow through a row of bluff bodies. *J. Fluid Mech.* **257**, 421–449.

Elcrat, A., Fornberg, B., Horn, M. & Miller, K. 2000 Some steady vortex flows past a circular cylinder. *J. Fluid Mech.* **409**, 13–27.

Elcrat, A. & Miller, K. 2001 A monotone iteration for concentrated vortices. *Nonlinear Analysis* (to appear).

Fornberg, B. 1988 Steady viscous flow past a sphere at high Reynolds numbers. *J. Fluid Mech.* **190**, 471–489.

Hill, M. 1894 On a spherical vortex. *Phil. Trans. R. Soc. Lond.* A **185**, 213–245.

Norbury, J. 1972 A steady vortex ring close to Hill's spherical vortex. *Proc. Camb. Phil. Soc.* **72**, 253–284.

Norbury, J. 1973 A family of steady vortex rings. *J. Fluid Mech.* **57**, 417–431.

Peregrine, D. 1985 A note on the steady high-Reynolds-number flow about a circular cylinder. *J. Fluid Mech.* **157**, 493–500.

Pozrikidis, C. 1986 The nonlinear instability of Hill's vortex. *J. Fluid Mech.* **168**, 337–367.

Saffman, P. 1981 Dynamics of vorticity. *J. Fluid Mech.* **106**, 49–58.

Saffman, P. 1992 *Vortex Dynamics*. Cambridge University Press.

Smith, F. T. 1985 A structure for laminar flow past a bluff body at high Reynolds number. *J. Fluid Mech.* **155**, 179–191.